

# Micromechanics-based elastic model for functionally graded materials with particle interactions

H.M. Yin <sup>a</sup>, L.Z. Sun <sup>a,\*</sup>, G.H. Paulino <sup>b</sup>

<sup>a</sup> Department of Civil and Environmental Engineering and Center for Computer-Aided Design, The University of Iowa, Iowa City, IA 52242, USA

<sup>b</sup> Department of Civil and Environmental Engineering, Newmark Laboratory, University of Illinois at Urbana-Champaign, Urbana, IL 61801, USA

Received 9 October 2003; received in revised form 6 April 2004; accepted 8 April 2004

Available online 6 May 2004

## Abstract

A micromechanics-based elastic model is developed for two-phase functionally graded materials with locally pair-wise interactions between particles. While the effective material properties change gradually along the gradation direction, there exist two microstructurally distinct zones: particle–matrix zone and transition zone. In the particle–matrix zone, pair-wise interactions between particles are employed using a modified Green's function method. By integrating the interactions from all other particles over the representative volume element, the homogenized elastic fields are obtained. The effective stiffness distribution over the gradation direction is further derived. In the transition zone, a transition function is constructed to make the homogenized elastic fields continuous and differentiable in the gradation direction. The model prediction is compared with other models and experimental data to demonstrate the capability of the proposed method.

© 2004 Acta Materialia Inc. Published by Elsevier Ltd. All rights reserved.

**Keywords:** Functionally graded materials; Composites; Micromechanical modeling; Elastic behavior; Pair-wise interaction

## 1. Introduction

In recent years functionally graded materials (FGMs) have attracted a good deal of attention from engineers and researchers due to their unique thermomechanical performance [1–3]. These materials are characterized for spatially varying microstructures created by non-uniform distributions of the reinforcement phase, as well as by interchanging the role of the reinforcement and matrix in a continuous manner [4]. Within FGMs, the different microstructural phases have different functions, and the overall FGMs attain the multifunctional status from their property gradation, enabling various multifunctional tasks by virtue of spatially tailored microstructures. For instance, in a ceramic/metal FGM, a continuous trade-off of metallic toughness and high thermal conductivity is made with ceramic hardness and

low thermal conductivity. In heat and impact protection applications, the material multifunctionality consists of the ability to provide structural support by virtue of the metallic portions of the FGM, and the simultaneous ability of the same material system to provide the required thermal or impact resistance by virtue of the ceramic portions of the FGM.

Several FGMs are manufactured by two phases of materials with different properties. Since the volume fraction of each phase gradually varies in the gradation direction, the effective properties of FGMs change along this direction. While FGMs have been designed and fabricated by diverse methods to achieve unique microstructures, very limited analytical investigations are available to tackle the spatial variation of microstructure [5]. Conventional composite models such as the Mori–Tanaka method [6] and the self-consistent method [7,8] are directly applied to estimate the effective elastic responses of FGMs [1,2,9–12]. Because they were originally developed for homogeneous mixtures with constant particle concentration, those models are not able to capture the material gradient nature of FGMs. Fur-

\* Corresponding author. Tel.: +1-319-384-0830; fax: +1-319-335-5660.

E-mail address: [lizhi-sun@uiowa.edu](mailto:lizhi-sun@uiowa.edu) (L.Z. Sun).

thermore, no direct interactions between particles are taken into consideration [13].

Experimental observations (e.g., [3,14]) show that the typical microstructure of FGMs, illustrated in Fig. 1(a) towards the gradation direction, contains a particle–matrix zone with discrete particles filled in continuous matrix, followed by a skeletal transition zone in which the particle and matrix phases cannot be well defined because the two phases are interpenetrated into each other as a connected network. The transition zone is further followed by another particle–matrix zone with interchanged phases of particle and matrix. Hirano et al. [15] applied the fuzzy logic approach to estimate the effective elastic behavior in the transition zone by using a transition function to combine the two solutions obtained from the particle–matrix zones. Reiter and Dvorak [16] also adopted the transition functions combined with the Mori–Tanaka model in the particle–matrix zone and self-consistent model in the skeletal transition zone.

The above-mentioned FGMs models did not directly include the local interactions between particles. Consequently, they could not take into account the graded particle distribution for FGMs. Some studies have suggested the need for higher order theory in the modeling of FGMs. For example, Zuiker and Dvorak [17] extended the Mori–Tanaka method to linearly varying

fields and investigated the relations of the averaged stress versus strain relation and of the stress-gradient versus strain-gradient, which was shown to be dependent on the size of the representative volume element (RVE). Here the RVE for a material point in a continuum body is a material volume that statistically represents the material neighborhood of the material point [24]. Aboudi et al. [5] developed a higher-order numerical cell theory based on volumetric averaging of the various fields. Micromechanical finite element models have also been constructed [16,18–20]. While taking into account the local particle interactions, these numerical methods are computationally intensive and inconvenient to be implemented for engineering structural analysis.

In this paper a micromechanical framework is proposed to investigate the effective elastic behavior of FGMs. Based on the Eshelby's equivalent inclusion method [21], the pair-wise particle interaction is collected for any two particles embedded in the matrix medium. Given a uniform loading on the upper and lower boundaries of FGMs, averaged strains in particles are derived by integrating pair-wise interaction contributions of all particles. In the course of derivation, the microscopic RVE is constructed to reflect the microstructure of FGMs. A transition function is adopted in the skeletal transition zone. From the effective stress and strain fields distributed in the gradation direction of FGMs, the effective elasticity distribution is solved as a function of gradation direction.

The rest of this paper is organized as follows. In Section 2, we briefly review the Eshelby's equivalent inclusion method [21] and two-inhomogeneity interaction in the infinite medium [22]. We then apply the pair-wise particle interaction for the micromechanical analysis of FGMs to develop an elastic constitutive model in Section 3. We further discuss the relation of the proposed model and the Mori–Tanaka model, and present the numerical results and comparisons with available experimental data in Section 4.

## 2. Micromechanics of pair-wise particle interaction

To solve the local elastic field of a single ellipsoidal particle filled in the infinite domain under a far field strain, Eshelby [21] offered an analytical solution through a so-called equivalent inclusion method. The essence of this method is that the particle–matrix heterogeneous domain is transferred to a homogeneous domain same as the matrix material but with an eigen-strain acting in the particle phase to represent inhomogeneity. The equivalent inclusion method has been widely applied in evaluating the effective mechanical properties of heterogeneous composites [23,24].

Based on the Eshelby's equivalent inclusion method, the local strain field at a certain point  $\mathbf{x}$  for one particle

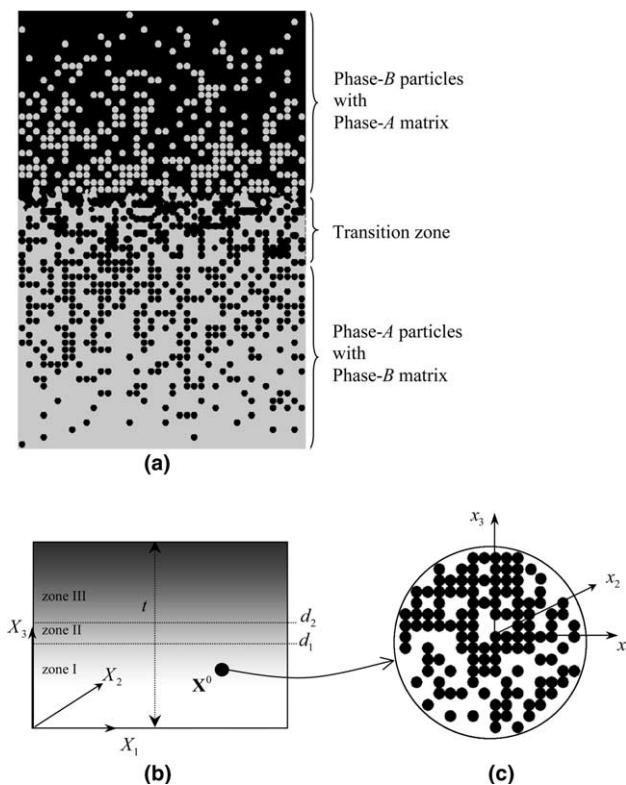


Fig. 1. Schematic illustration of a two-phase FGM sample: (a) typical microstructure including A and B phases; (b) three zones in macro scale  $\mathbf{X}$ ; and (c) RVE in the microscopic scale  $\mathbf{x}$ .

with the radius  $a$  embedded in the infinite matrix under the external far-field strain  $\boldsymbol{\varepsilon}^0$  can be written as

$$\boldsymbol{\varepsilon}(\mathbf{x}) = \boldsymbol{\varepsilon}^0 + \boldsymbol{\varepsilon}'(\mathbf{x}), \quad (1)$$

where the perturbed strain  $\boldsymbol{\varepsilon}'$  due to the elastic mismatch between the particle and the matrix reads:

$$\boldsymbol{\varepsilon}'(\mathbf{x}) = - \int_{\Omega} \boldsymbol{\Gamma}(\mathbf{x}, \mathbf{x}') \cdot \mathbf{C}_0 : \boldsymbol{\varepsilon}^*(\mathbf{x}') d\mathbf{x}', \quad (2)$$

in which  $\Omega$  represents the ellipsoidal particle domain in general,  $\mathbf{C}_0$  signifies the elastic stiffness tensor of the matrix, and  $\boldsymbol{\varepsilon}^*$  denotes the equivalent eigenstrain. The symbols “ $\cdot$ ” and “ $:$ ” indicate the tensor contraction between two fourth-rank tensors and between fourth-rank and second-rank tensors, respectively. The modified two-point Green function  $\boldsymbol{\Gamma}$  has the explicit form as [25]:

$$\begin{aligned} \Gamma_{ijkl}(\mathbf{x}, \mathbf{x}') = & \frac{1}{16\pi\mu_0(1-v_0)r^3} [\delta_{ij}\delta_{kl} - (1-2v_0) \\ & \times (\delta_{ik}\delta_{jl} + \delta_{il}\delta_{jk}) - 3(\delta_{ij}n_k n_l + \delta_{kl}n_i n_j) \\ & - 3v_0(\delta_{ik}n_j n_l + \delta_{jk}n_i n_l + \delta_{il}n_j n_k + \delta_{jl}n_i n_k) \\ & + 15n_i n_j n_k n_l], \end{aligned} \quad (3)$$

with  $r = |\mathbf{x} - \mathbf{x}'|$ ,  $\mathbf{n} = (\mathbf{x} - \mathbf{x}')/r$ , and  $\mu_0$  and  $v_0$  being the shear modulus and Poisson’s ratio of the matrix, respectively.

From the stress equivalent formulation in the spherical particle domain with elastic stiffness  $\mathbf{C}_1$

$$\mathbf{C}_1 : [\boldsymbol{\varepsilon}^0 + \boldsymbol{\varepsilon}'(\mathbf{x})] = \mathbf{C}_0 : [\boldsymbol{\varepsilon}^0 + \boldsymbol{\varepsilon}'(\mathbf{x}) - \boldsymbol{\varepsilon}^*(\mathbf{x})], \quad (4)$$

the equivalent eigenstrain  $\boldsymbol{\varepsilon}^*$  is derived as

$$\boldsymbol{\varepsilon}^* = \mathbf{C}_0^{-1} \cdot (\mathbf{P}_0 - \Delta\mathbf{C}^{-1})^{-1} : \boldsymbol{\varepsilon}^0, \quad (5)$$

where  $\Delta\mathbf{C} = \mathbf{C}_1 - \mathbf{C}_0$ , and  $(P_0)_{ijkl} = [\delta_{ij}\delta_{kl} - (4-5v_0)(\delta_{ik}\delta_{jl} + \delta_{il}\delta_{jk})]/[30\mu_0(1-v_0)]$ . Combining Eqs. (1), (2) and (5), the local strain field can be calculated. In particular, the strain field  $\bar{\boldsymbol{\varepsilon}}$  in the spherical particle domain  $\Omega$  is shown to be uniform as

$$\bar{\boldsymbol{\varepsilon}} = (\mathbf{I} - \mathbf{P}_0 \cdot \Delta\mathbf{C})^{-1} : \boldsymbol{\varepsilon}^0, \quad (6)$$

with the fourth-rank identity tensor  $I_{ijkl} = (\delta_{ik}\delta_{jl} + \delta_{il}\delta_{jk})/2$ .

Moschovidis and Mura [22] extended the single particle problem to the case of two spherical particles with identical size embedded in the infinite matrix domain. By expanding the equivalent eigenstrain and the disturbing strain in terms of polynomial form of local coordinates, we can solve Eqs. (1), (2) and (4) for the local strain field  $\boldsymbol{\varepsilon}(\mathbf{x})$ . Furthermore, the averaged strain in each spherical particle domain  $\Omega$  is integrated as

$$\begin{aligned} \bar{\boldsymbol{\varepsilon}} & \stackrel{\Delta}{=} \frac{1}{V_{\Omega}} \int_{\Omega} \boldsymbol{\varepsilon}(\mathbf{x}) d\mathbf{x} \\ & = [\mathbf{I} - \mathbf{P}_0 \cdot \Delta\mathbf{C} - \mathbf{P}(\mathbf{x}_1, \mathbf{x}_2) \cdot \Delta\mathbf{C}]^{-1} : \boldsymbol{\varepsilon}^0 + \mathbf{O}(\tilde{\rho}^8), \end{aligned} \quad (7)$$

where  $\tilde{\rho} = a/b$  and  $V_{\Omega} = 4\pi a^3/3$  with  $a$  being the particle radius and  $b$  being the center-to-center distance between

the two particles centered at  $\mathbf{x}_1$  and  $\mathbf{x}_2$ , respectively. In addition, the fourth-rank tensor  $\mathbf{P}$  reads:

$$\begin{aligned} P_{ijkl}(\mathbf{x}_1, \mathbf{x}_2) = & \frac{\tilde{\rho}^3}{60\mu_0(1-v_0)} [(5\cdot\cdot - 3\tilde{\rho}^2)\delta_{ij}\delta_{kl} \\ & - (5 - 10v_0 + 3\tilde{\rho}^2)(\delta_{ik}\delta_{jl} + \delta_{il}\delta_{jk}) \\ & + 15(5 - 7\tilde{\rho}^2)\tilde{n}_i\tilde{n}_j\tilde{n}_k\tilde{n}_l - 15(1 - \tilde{\rho}^2) \\ & \times (\delta_{ij}\tilde{n}_k\tilde{n}_l + \delta_{kl}\tilde{n}_i\tilde{n}_j) - 15(v_0 - \tilde{\rho}^2) \\ & \times (\delta_{ik}\tilde{n}_j\tilde{n}_l + \delta_{jk}\tilde{n}_i\tilde{n}_l + \delta_{il}\tilde{n}_j\tilde{n}_k + \delta_{jl}\tilde{n}_i\tilde{n}_k)], \end{aligned} \quad (8)$$

with  $\tilde{\mathbf{n}} = (\mathbf{x}_1 - \mathbf{x}_2)/b$ . Comparing Eqs. (6) and (7), we can find that the additional particle provides an interaction on the averaged strain of the first particle as

$$\mathbf{d}(\mathbf{x}_1, \mathbf{x}_2) = \Delta\mathbf{C}^{-1} \cdot \mathbf{L}(\mathbf{x}_1, \mathbf{x}_2) : \boldsymbol{\varepsilon}^0, \quad (9)$$

where the pair-wise interaction tensor

$$\begin{aligned} \mathbf{L}(\mathbf{x}_1, \mathbf{x}_2) = & \left( [\Delta\mathbf{C}^{-1} - \mathbf{P}_0 - \mathbf{P}(\mathbf{x}_1, \mathbf{x}_2)]^{-1} - [\Delta\mathbf{C}^{-1} - \mathbf{P}_0]^{-1} \right) \\ & + \mathbf{O}(\tilde{\rho}^8). \end{aligned} \quad (10)$$

It is noted that the pair-wise interaction term can reach high precision as order of  $\mathbf{O}(\tilde{\rho}^8)$  where  $\tilde{\rho}$  is always no greater than 0.5. Further, the mathematical inverse operation of the fourth-rank tensor that appears in Eqs. (7) and (10) can be found in [13]. After lengthy but straightforward derivation, the fourth-rank pair-wise interaction tensor  $\mathbf{L}$  in Eq. (10) can be explicitly expressed as

$$\begin{aligned} L_{ijkl}(\mathbf{x}_1, \mathbf{x}_2) = & c_1\delta_{ij}\delta_{kl} + c_2(\delta_{ik}\delta_{jl} + \delta_{il}\delta_{jk}) \\ & + c_3(\delta_{ij}\tilde{n}_k\tilde{n}_l + \delta_{kl}\tilde{n}_i\tilde{n}_j) \\ & + c_4(\delta_{ik}\tilde{n}_j\tilde{n}_l + \delta_{il}\tilde{n}_j\tilde{n}_k + \delta_{jk}\tilde{n}_i\tilde{n}_l + \delta_{jl}\tilde{n}_i\tilde{n}_k) \\ & + c_5\tilde{n}_i\tilde{n}_j\tilde{n}_k\tilde{n}_l, \end{aligned} \quad (11)$$

where the coefficients  $c_i$  ( $i = 1, 2, \dots, 5$ ) are defined in Appendix A.

### 3. Micromechanical analysis of FGMs

Let us consider a typical FGM microstructure (Fig. 1) containing two phases A and B with isotropic elastic stiffness  $\mathbf{C}^A$  and  $\mathbf{C}^B$ , respectively. The global coordinate system of the FGM is denoted by  $(X_1, X_2, X_3)$  with  $X_3$  being the continuous gradation direction. The overall grading thickness of the FGM is  $t$ . In each infinitesimal graded layer ( $X_1$ - $X_2$  plane), micro-particles are uniformly distributed with a two-dimensionally random setting so that the material layer is statistically homogeneous. While these micro-particles cannot be observed in the macroscopic scale, the volume fraction of phase A or B (for convenience, we use  $\phi$  to denote the volume fraction of phase A) is gradually changed in the gradation direction  $X_3$ . Microscopically, the particle and the matrix zones could be well defined when  $\phi$  is close to 0 or 1 (e.g., Zone I

and Zone III in Fig. 1(b)). However, a skeletal transition zone (Zone II) normally exists in middle area (e.g.,  $d_1 < X_3 < d_2$ ) in which it is difficult to identify the particle or matrix phase. The transition zone boundaries  $d_1$  and  $d_2$  are generally determined by the FGM fabrication process directly related to the phase volume fraction  $\phi(X_3)$ .

To calculate the effective FGM elastic stiffness  $\bar{\mathbf{C}}(X_3)$ , a uniform far-field stress tensor  $\boldsymbol{\sigma}^0$  is first applied on the FGM  $X_3$  boundary. Based on the equilibrium condition, the far-field stress should be related to the averaged strain  $\langle \boldsymbol{\varepsilon} \rangle(X_3)$  in each  $X_1$ – $X_2$  layer as

$$\boldsymbol{\sigma}^0 = \bar{\mathbf{C}}(X_3) : \langle \boldsymbol{\varepsilon} \rangle(X_3), \quad (12)$$

where the far-field stress (equal to the averaged stress  $\langle \boldsymbol{\sigma} \rangle(X_3)$ ) and averaged strain in the  $X_1$ – $X_2$  layer can be further written as

$$\boldsymbol{\sigma}^0 = \phi(X_3)\mathbf{C}^A : \langle \boldsymbol{\varepsilon} \rangle^A(X_3) + [1 - \phi(X_3)]\mathbf{C}^B : \langle \boldsymbol{\varepsilon} \rangle^B(X_3), \quad (13)$$

$$\langle \boldsymbol{\varepsilon} \rangle(X_3) = \phi(X_3)\langle \boldsymbol{\varepsilon} \rangle^A(X_3) + [1 - \phi(X_3)]\langle \boldsymbol{\varepsilon} \rangle^B(X_3). \quad (14)$$

For any macroscopic material point  $\mathbf{X}^0$  (Fig. 1(b)) in the range of  $0 \leq X_3 \leq d_1$  (Zone I), the corresponding microstructural RVE (Fig. 1(c)) contains a number of micro-particles of the phase A embedded in a continuous matrix of the phase B so that the overall volume fraction of particle phase A and the its gradient should be consistent with the macroscopic counterparts  $\phi(X_3^0)$  and  $d\phi/dX_3|_{X_3=X_3^0}$ . The microscopic coordinate system ( $x_1, x_2$ , and  $x_3$ ) is constructed with the origin corresponding to  $\mathbf{X}^0$ . All micro-particles are assumed to be specifically spherical with identical radius  $a$  ( $a \ll t$ ) for straightforward formulation. The whole RVE domain is denoted as  $D$  and the  $i$ th micro-particle ( $i = 1, 2, 3, \dots, \infty$ ) domain is denoted as  $\Omega_i$  centered at  $\mathbf{x}^i$ . For the ease of formulation, a particle centered at the origin is assumed and denoted as  $\Omega_0$ .

While the Eshelby's single spherical-particle solution offers the uniform strain distribution in the particle phase, the local strain field in each particle is position-dependent for many particles embedded in the matrix. To simplify the elastic modeling for the FGM, the averaged particle strains are collected based on the local strain fields in particles located at various  $x_1$ – $x_2$  layers. Specifically, the averaged strain in the central particle  $\Omega_0$  can be written in two parts: the elastic-mismatch interaction between the central particle and the matrix (Eq. (6)) and the pair-wise interaction between the central particle and other particles (Eq. (9)):

$$\langle \boldsymbol{\varepsilon} \rangle^A(\mathbf{0}) = (\mathbf{I} - \mathbf{P}_0 \cdot \Delta\mathbf{C})^{-1} : \langle \boldsymbol{\varepsilon} \rangle^B(\mathbf{0}) + \sum_{i=1}^{\infty} \Delta\mathbf{C}^{-1} \cdot \mathbf{L}(\mathbf{0}, \mathbf{x}^i) \langle \boldsymbol{\varepsilon} \rangle^B(x_3^i), \quad (15)$$

where  $\langle \boldsymbol{\varepsilon} \rangle^B(\mathbf{0})$  is the averaged matrix strain in the layer with  $x_3 = 0$  and  $\langle \boldsymbol{\varepsilon} \rangle^B(x_3^i)$  is the averaged matrix strain tensor in the  $x_3^i$ th layer. Because all particles are statistically distributed in a random way, the probability of

particle distribution can be introduced to statistically demonstrate the particle interaction effect. Therefore, the second-rank pair-wise interaction tensor  $\langle \mathbf{d} \rangle(\mathbf{0})$  (i.e., the second term of the right hand side of Eq. (15)) can be further integrated over all possible particle positions as

$$\langle \mathbf{d} \rangle(\mathbf{0}) \triangleq \sum_{i=1}^{\infty} \Delta\mathbf{C}^{-1} \cdot \mathbf{L}(\mathbf{0}, \mathbf{x}^i) : \langle \boldsymbol{\varepsilon} \rangle^B(x_3^i) = \int_D P(\mathbf{x}|\mathbf{0}) \Delta\mathbf{C}^{-1} \cdot \mathbf{L}(\mathbf{0}, \mathbf{x}) : \langle \boldsymbol{\varepsilon} \rangle^B(x_3) d\mathbf{x}, \quad (16)$$

where  $P(\mathbf{x}|\mathbf{0})$  is the conditional number density function used to find a particle centered at  $\mathbf{x}$  when the first particle is located at  $\mathbf{0}$ . For statistically homogeneous composite materials containing randomly distributed spherical particles with the volume fraction  $\phi$ , the particle probability density function is frequently proposed as [13,26]:

$$P(\mathbf{x}|\mathbf{0}) = \frac{3\phi g(x)}{4\pi a^3}, \quad (17)$$

where  $x$  denotes the distance from  $\mathbf{x}$  to  $\mathbf{0}$ , or  $|\mathbf{x}|$ . The term  $3\phi/(4\pi a^3)$  in fact indicates the total number of particles per unit volume. The other term  $g(x)$  is the radial distribution function of particles proposed by Percus and Yevick [27] to estimate the particle non-uniformity effect in the radial direction.

For the FGM considered, since the micro-particles in RVE are distributed in a continuously increasing manner in the gradation direction, the particle density function is proposed as

$$P(\mathbf{x}|\mathbf{0}) = \frac{3g(x)}{4\pi a^3} [\phi(X_3^0) + e^{-x/\delta} \phi_{,3}(X_3^0)x_3]. \quad (18)$$

Here the expression enclosed by square brackets is constructed on the basis that the averaged volume fraction of particle in the RVE is  $\phi(X_3^0)$ , the gradient of particle volume fraction is  $\phi_{,3}(X_3^0)$ , and in the far field the particle concentration must not be beyond the range of zero to the maximum particle concentration. Thus, an exponential function is introduced to attenuate the gradation term exponentially. The parameter  $\delta$ , which controls the attenuating rate, will be determined under the condition that the maximum volume fraction of particles in the RVE should not be greater than the maximum volume fraction in particle–matrix zone. Since the particle interaction energy is quickly attenuated with the increment of the distance between particles, those particles in the neighboring domain of the central particle should contribute the majority part for the averaged strain of the central particle.

Similarly to Moschovidis and Mura [22] and Ju and Chen [13], the Taylor expansion of  $\langle \boldsymbol{\varepsilon} \rangle^B(x_3)$  is applied to analytically integrate equation (16). It is noted that the average strain  $\langle \boldsymbol{\varepsilon} \rangle^B(x_3)$  varies along the grading direction. It is differentiable and bounded, and thus is approximated by the Taylor expansion. In the chosen

RVE, the elastic interaction between the central particle and the particles far away from it is negligible; only the particles in the close neighborhood of the central particle may have noticeable interaction on the central particle. As a first order approximation, we truncate the Taylor expansion of  $\langle \boldsymbol{\varepsilon} \rangle^B(x_3)$  to linear term in terms of  $x_3$  so that Eq. (16) can be analytically integrated and rewritten as

$$\langle \mathbf{d} \rangle(\mathbf{0}) = \phi(X_3^0) \Delta \mathbf{C}^{-1} \cdot \mathbf{D}(\mathbf{0}) : \langle \boldsymbol{\varepsilon} \rangle^B(\mathbf{0}) + \phi_{,3}(X_3^0) \Delta \mathbf{C}^{-1} \cdot \mathbf{F}(\mathbf{0}) : \langle \boldsymbol{\varepsilon} \rangle_{,3}^B(\mathbf{0}), \quad (19)$$

where

$$\mathbf{D} = \int_D \frac{3g(x)}{4\pi a^3} \mathbf{L}(\mathbf{0}, \mathbf{x}) d\mathbf{x}, \quad (20)$$

$$\mathbf{F} = \int_D e^{-x/\delta} \frac{3g(x)}{4\pi a^3} \mathbf{L}(\mathbf{0}, \mathbf{x}) x_3^2 d\mathbf{x}.$$

The above two integration terms  $\mathbf{D}$  and  $\mathbf{L}$  can be further simplified. The volume element  $d\mathbf{x} = dx_1 dx_2 dx_3$  can be expressed as  $d\mathbf{x} = x^2 d\omega dx$  where  $x \triangleq |\mathbf{x}|$  and  $d\omega$  is the surface element on the unit sphere  $\Sigma$  centered at the origin of the coordinates.

With the help of the following identities

$$\int_{\Sigma} \tilde{n}_i \tilde{n}_j d\omega = \frac{4\pi}{3} \delta_{ij}, \quad (21)$$

$$\int_{\Sigma} \tilde{n}_i \tilde{n}_j \tilde{n}_k \tilde{n}_l d\omega = \frac{4\pi}{15} (\delta_{ij} \delta_{kl} + \delta_{ik} \delta_{jl} + \delta_{il} \delta_{jk}) \quad (22)$$

and

$$\int_{\Sigma} \tilde{n}_i \tilde{n}_j \tilde{n}_k \tilde{n}_l \tilde{n}_p \tilde{n}_q d\omega = \frac{4\pi}{105} [\delta_{ij} (\delta_{kl} \delta_{pq} + \delta_{kp} \delta_{lq} + \delta_{kq} \delta_{lp}) + \delta_{ik} (\delta_{jl} \delta_{pq} + \delta_{jp} \delta_{lq} + \delta_{jq} \delta_{lp}) + \delta_{il} (\delta_{jk} \delta_{pq} + \delta_{jp} \delta_{kq} + \delta_{jq} \delta_{kp}) + \delta_{ip} (\delta_{jk} \delta_{lq} + \delta_{jl} \delta_{kq} + \delta_{jq} \delta_{kl}) + \delta_{iq} (\delta_{jk} \delta_{lp} + \delta_{jl} \delta_{kp} + \delta_{jp} \delta_{kl})], \quad (23)$$

the two integrations can be further simplified as

$$\int_{\Sigma} L_{ijkl}(\mathbf{0}, \mathbf{x}) d\omega = \frac{4\pi}{15} (15c_1 + 10c_3 + c_5) \delta_{ij} \delta_{kl} + \frac{4\pi}{15} (15c_2 + 10c_4 + c_5) (\delta_{ik} \delta_{jl} + \delta_{il} \delta_{jk}) \quad (24)$$

and

$$\int_{\Sigma} L_{ijkl}(\mathbf{0}, \mathbf{x}) \tilde{n}_3^2 d\omega = \frac{4\pi}{105} [35c_1 + 14c_3 + c_5 + 2(7c_3 + c_5)(\delta_{l3} + \delta_{k3})] \delta_{ij} \delta_{kl} + \frac{4\pi}{105} [35c_2 + 14c_4 + c_5 + 2(7c_4 + c_5)(\delta_{l3} + \delta_{j3})] (\delta_{ik} \delta_{jl} + \delta_{il} \delta_{jk}). \quad (25)$$

It is noted that Mura's [23] tensorial indicial notation is followed in the above equation; i.e., uppercase indices have the same representation as the corresponding lowercase ones but are not summed. Recognizing the explicit form of Eqs. (24) and (25), only one-dimensional numerical integration in terms of  $x$  should be further employed to calculate  $\mathbf{D}$  and  $\mathbf{F}$  in Eq. (20).

Substituting Eq. (19) into Eq. (15) and recognizing that the origin of the local coordinates in the RVE corresponds to the global coordinate point  $\mathbf{X}^0$  of FGM, we can obtain the averaged particle strain tensor in terms of the arbitrary material point  $X_3$

$$\langle \boldsymbol{\varepsilon} \rangle^A(X_3) = (\mathbf{I} - \mathbf{P}_0 \cdot \Delta \mathbf{C})^{-1} : \langle \boldsymbol{\varepsilon} \rangle^B(X_3) + \phi(X_3) \Delta \mathbf{C}^{-1} \cdot \mathbf{D}(X_3) : \langle \boldsymbol{\varepsilon} \rangle^B(X_3) + \phi_{,3}(X_3) \Delta \mathbf{C}^{-1} \cdot \mathbf{F}(X_3) : \langle \boldsymbol{\varepsilon} \rangle_{,3}^B(X_3). \quad (26)$$

With the combination of Eqs. (13) and (26), the averaged particle strain tensor  $\langle \boldsymbol{\varepsilon} \rangle^A(X_3)$  and the averaged matrix strain tensor  $\langle \boldsymbol{\varepsilon} \rangle^B(X_3)$  in the FGM gradation direction  $X_3$  can be solved in terms of the far-field stress  $\boldsymbol{\sigma}^0$ . Since Eq. (26) is a set of ordinary differential equations, we also need the appropriate boundary conditions. In the particle–matrix zone with  $0 \leq X_3 \leq d_1$ , the boundary at  $X_3 = 0$  corresponds to the 100% matrix material (i.e.,  $\phi(0) = 0$ ). The corresponding boundary conditions can be proposed as

$$\langle \boldsymbol{\varepsilon} \rangle^B(\mathbf{0}) = \mathbf{C}^{B-1} : \boldsymbol{\sigma}^0. \quad (27)$$

Therefore, the averaged strain tensors in both phases can be numerically solved on the basis of standard backward Eulerian method. Similarly, in the other particle–matrix with the range of  $d_2 \leq X_3 \leq t$  (zone III), we can also calculate the averaged strain fields by the switch of matrix and particle phases. It is noted that, for those FGMs of which the volume fraction of phase A does not start from 0% (say 10%), the boundary condition equation (27) is no longer valid. The modified boundary condition of  $\langle \boldsymbol{\varepsilon} \rangle^B(\mathbf{0})$  can be obtained from the combination of Eqs. (12)–(14) for  $X_3 = 0$  where the composite elastic properties  $\bar{\mathbf{C}}(\mathbf{0})$  (i.e., 10% phase A and 90% phase B) at the boundary are estimated with the help of conventional composite models such as the Mori–Tanaka model [6] or self-consistent model [7,8].

For the transition zone II ( $d_1 < X_3 < d_2$ ), the particle and matrix phases cannot be well defined because the two phases are interpenetrated into each other as a connected network. As a consequence, the averaged elastic fields cannot explicitly be determined through the micromechanics framework. Similarly to Reiter and Dvorak [16], a phenomenological transition function is introduced as

$$f(X_3) = \left[ 1 - 2 \frac{\phi(X_3) - \phi(d_1)}{\phi(d_1) - \phi(d_2)} \right] \left[ \frac{\phi(X_3) - \phi(d_2)}{\phi(d_1) - \phi(d_2)} \right]^2, \quad (28)$$

so that the averaged strain of each phase (A or B) in the transition zone II can be approximated as a cubic Hermite function appropriately contributed by the averaged strain of the same phase (A or B) from two particle–matrix zones (zones I and III). Namely,

$$\langle \boldsymbol{\varepsilon} \rangle_{\text{zone-II}}^{\text{A or B}}(X_3) = f(X_3) \langle \boldsymbol{\varepsilon} \rangle_{\text{zone-I}}^{\text{A or B}}(X_3) + [1 - f(X_3)] \langle \boldsymbol{\varepsilon} \rangle_{\text{zone-III}}^{\text{A or B}}(X_3). \quad (29)$$

The overall averaged strain tensor at each layer in the transition zone can be further obtained from Eq. (14). It is noted that the proposed transition function satisfies the requirement that the effective FGM elastic fields and corresponding moduli should be bounded, continuous, and differentiable [28].

Given a specifically uniaxial loading  $\sigma_{33}^0$  on the lower and upper FGM boundaries, from Eq. (12), the effective Young's modulus and the Poisson's ratio at any material layer in the FGM gradation direction can be derived as

$$E(X_3) = \frac{\sigma_{33}^0}{\langle \varepsilon_{33} \rangle(X_3)}; \quad \nu(X_3) = -\frac{\langle \varepsilon_{11} \rangle(X_3)}{\langle \varepsilon_{33} \rangle(X_3)}. \quad (30)$$

The effective shear modulus at any material layer in the gradation direction can be similarly obtained through an applied shear loading  $\tau_{13}^0$  as

$$\mu(X_3) = \frac{\tau_{13}^0}{2\langle \varepsilon_{13} \rangle(X_3)}. \quad (31)$$

#### 4. Numerical simulations and discussion

From the above procedures, when a uniformly distributed loading is applied on the FGM upper and lower boundaries, the effective Young's modulus, Poisson's ratio and shear modulus distributions over the FGM can be estimated. Since most two-phase FGMs are fabricated to gradually change material phases from one end to the other, the effective elastic properties strongly depend on the individual performance of constituent phases. The effect of phase modulus contrast on the overall FGM elastic behavior is shown in Fig. 2. Specifically, the effective Young's modulus (Fig. 2(a)) in the FGM gradation direction increases as the volume fraction of phase A increases, ranging from Zone I (phase A as particle phase), Zone II (transition zone), and Zone III (phase A as matrix phase). Continuous and differentiable jump is expected in the transition zone II when the phase modulus contrast ratio is large. Unless otherwise stated, the lower and upper bounds  $d_1$  and  $d_2$  are conveniently selected where the corresponding volume fractions are 40% and 60%, respectively, which follows Bao and Cai's suggestion [29]. It is suggested that the larger transition zone made during FGM fabrication is desirable to prevent the significant jump of effective elasticity when the elastic contrast ratio is big.

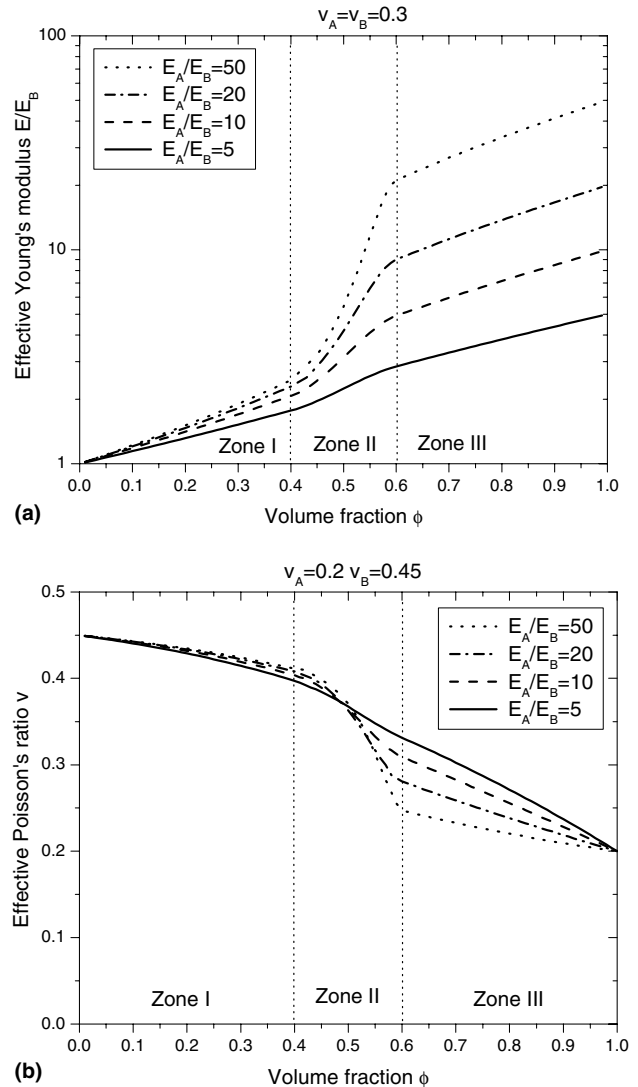
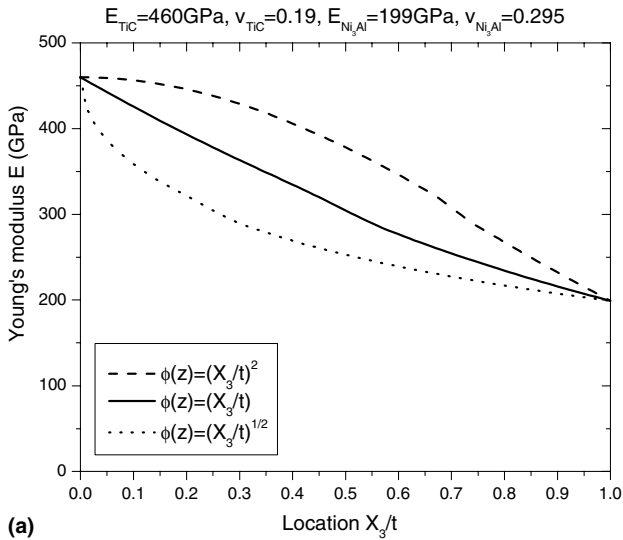


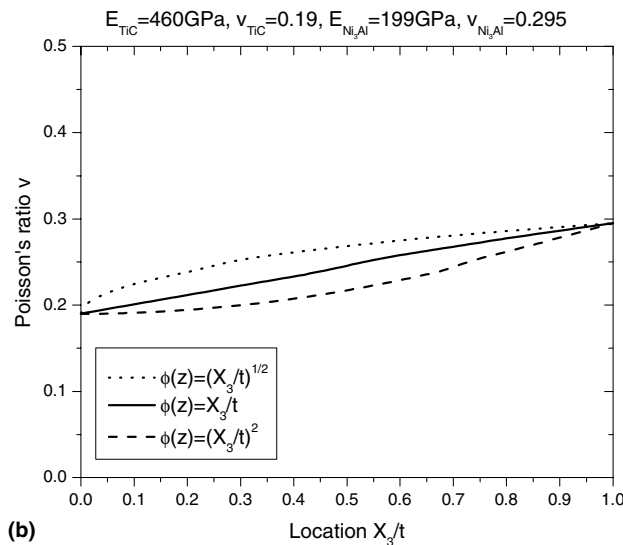
Fig. 2. Effect of modulus contrast ratio on (a) the effective FGM Young's modulus and (b) the effective FGM Poisson's ratio.

While the effective Poisson's ratio (Fig. 2(b)) varies between the Poisson's ratios of individual phases and depends on the phase modulus contrast, it is not as significant as the effective modulus of FGMs.

Changing the phase volume fraction distribution also affects the elastic responses of FGMs. Fig. 3 illustrates the effective Young's modulus and the Poisson's ratio distribution as a function of three types of volume fraction distribution cases (quadratic, linear, and square-root cases). The FGM material includes TiC as phase A and  $\text{Ni}_3\text{Al}$  as phase B. Their elastic parameters are obtained from [30] as:  $E_{\text{TiC}} = 460$  GPa,  $\nu_{\text{TiC}} = 0.19$ ,  $E_{\text{Ni}_3\text{Al}} = 199$  GPa and  $\nu_{\text{Ni}_3\text{Al}} = 0.295$ . The transition zone is bounded as  $\phi(d_1) = 40\%$  and  $\phi(d_2) = 60\%$ . It is shown from Fig. 3 that the effective Young's modulus of the TiC– $\text{Ni}_3\text{Al}$  FGM is in the range of  $E_{\text{Ni}_3\text{Al}}$  to  $E_{\text{TiC}}$ , and effective Poisson's ratio in the range of  $\nu_{\text{Ni}_3\text{Al}}$  to  $\nu_{\text{TiC}}$  as expected. However, at a given location, the effective



(a)



(b)

Fig. 3. Effect of phase volume fraction distribution on (a) the effective FGM Young's modulus and (b) the effective FGM Poisson's ratio.

elastic responses are strongly dependent on the phase volume fraction distribution, suggesting that the overall mechanical behavior can be tailored through phase distribution pattern for desired FGM material design.

Conventional micromechanics-based FGM models (e.g., Mori–Tanaka method and self-consistent method) do not directly take into account the local particle interactions and gradient effects of phase volume fractions. On the contrary, our proposed model adopts the pair-wise local interaction between particles and includes the deformation gradient in the micromechanics framework. Therefore, our elastic prediction depends not only on the phase volume fraction, but on the gradient of volume fraction as well. More specifically, the second term of the right-hand side in Eq. (26) denotes the pair-wise interaction contribution while the third term represents the gradient effect. If these two terms are

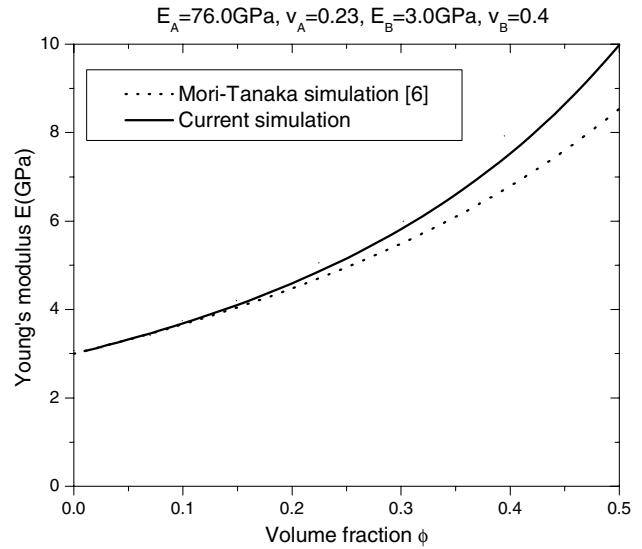


Fig. 4. Comparisons of effective glass-epoxy FGM Young's moduli between the proposed model simulations and Mori–Tanaka method [6].

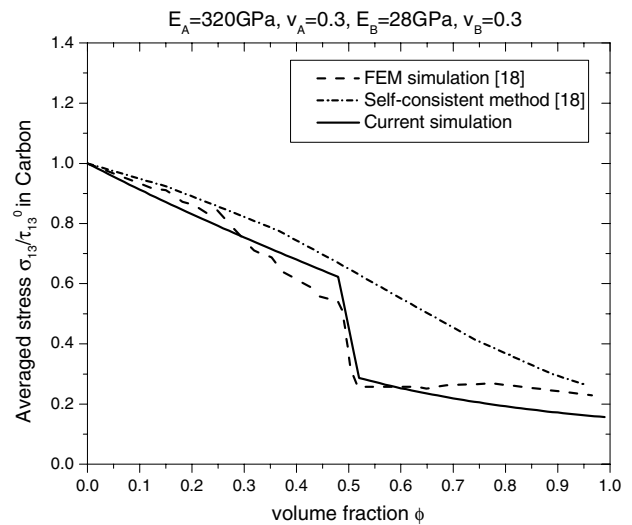


Fig. 5. Comparisons of averaged shear stress distribution among the proposed model, self-consistent method [18], and finite element method (FEM) [18].

dropped from the equation, then the proposed model recovers the standard Mori–Tanaka's model. Fig. 4 shows the simulation comparison between the proposed particle interaction model and conventional Mori–Tanaka model. In a certain FGM zone I ranging from  $0 \leq \phi \leq 50\%$  with glass particles ( $E_A = 76$  GPa,  $\nu_A = 0.23$ ) embedded in the epoxy matrix ( $E_B = 3.0$  GPa,  $\nu_B = 0.40$ ), Mori–Tanaka method underestimates the effective elastic response when the phase volume fraction exceeds 20%. Furthermore, the proposed model is compared with self-consistent method and finite element method (FEM) both performed by Reiter et al. [18] as illustrated in Fig. 5. It is shown that, when the

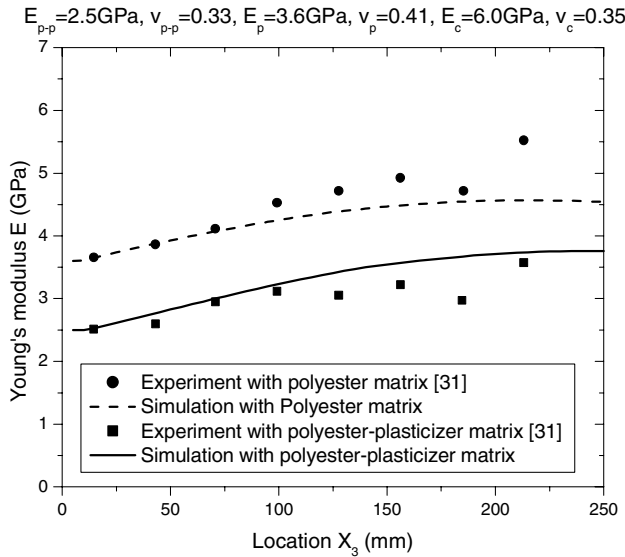


Fig. 6. Comparisons of effective FGM Young's moduli between the proposed model simulations and experimental data [31].

shear traction  $\tau_{13}^0$  is applied on the upper boundary of a C/SiC FGM with the carbon as phase A ( $E_A = 28$  GPa,  $v_A = 0.3$ ) and the silicon carbide as phase B ( $E_B = 320$  GPa,  $v_B = 0.3$ ), averaged shear stress on the carbon phase estimated by the current model is much closer to the numerical FEM results than the one estimated by the self-consistent method. The transition zone is taken from  $\phi(d_1) = 48\%$  to  $\phi(d_1) = 52\%$  to be consistent with FEM simulation [18].

Elastic simulations from the proposed model are also compared with available experimental data to demonstrate the validity of the micromechanics-based particle interaction model. One such comparison is illustrated in

Fig. 6. The experimental data were provided in [31] with two types of FGM fabrications: cenospheres in the polyester matrix and cenospheres in the polyester-plasticizer matrix. The cenospheres are hollow spheres made of aluminum silicates with the mean diameter of  $127 \mu\text{m}$  and wall thickness of  $12.7 \mu\text{m}$ . During the simulation process, the hollow spheres are replaced by solid particles with the estimated Young's modulus and Poisson's ratio as  $E_c = 6.0$  GPa and  $v_c = 0.35$ . The particle volume fractions vary continuously from 0% to 45% with the particle concentration distributions in the gradation direction  $X_3$  given as:  $\phi(X_3) = -0.4731 + 4.226 \times 10^{-3}X_3 - 8.666 \times 10^{-6}X_3^2$  for cenospheres in the polyester matrix and  $\phi(X_3) = -0.3729 + 4.561 \times 10^{-3}X_3 - 1.06 \times 10^{-5}X_3^2$  for the polyester-plasticizer matrix, respectively. The thickness of the two FGMs is 250 mm ( $0 \leq X_3 \leq 250$  mm). The phase Young's moduli and Poisson's ratios are given as:  $E_p = 3.6$  GPa,  $v_p = 0.41$ ,  $E_{p-p} = 2.5$  GPa,  $v_{p-p} = 0.33$  with the subscript 'p' denoting the polyester matrix and 'p-p' representing the polyester-plasticizer matrix. With these parameters as input data, the effective Young's moduli of the FGMs are simulated and shown in Fig. 6 as a function of location in the gradation direction. The proposed model compares well with the experimental results.

Zhai et al. [30] conducted the effective elastic properties of TiC/Ni<sub>3</sub>Al FGM with phase material properties as  $E_{\text{TiC}} = 460$  GPa,  $v_{\text{TiC}} = 0.19$ ,  $E_{\text{Ni}_3\text{Al}} = 199$  GPa and  $v_{\text{Ni}_3\text{Al}} = 0.295$ . Fig. 7 shows the comparisons between the proposed model with the linear volume fraction distribution and the experiment data for both effective Young's modulus (Fig. 7(a)) and Poisson's ratio (Fig. 7(b)). The transition zone is included with the lower and upper bounds  $d_1$  and  $d_2$  selected corresponding to the volume fractions of 40% and 60%, respectively.

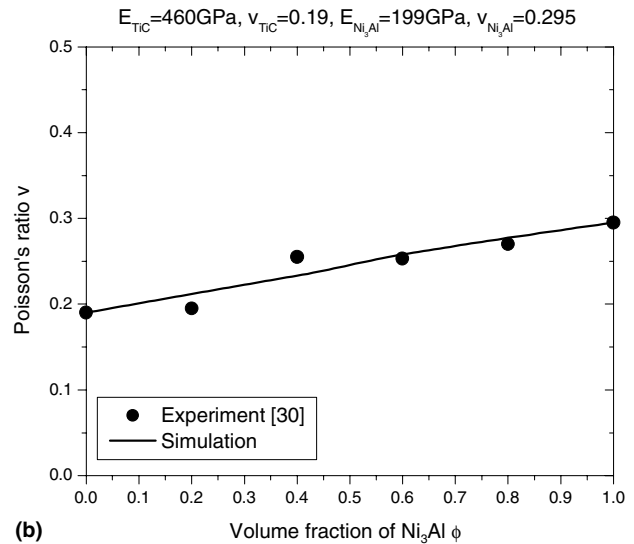
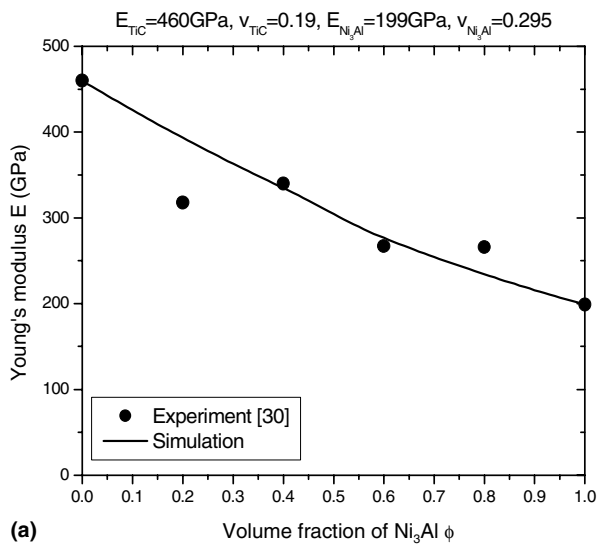


Fig. 7. Comparisons between the proposed model simulations and experimental data [30]; (a) the effective FGM Young's modulus vs. phase volume fraction and (b) the effective FGM Poisson's ratio vs. phase volume fraction.

## 5. Conclusions

In this paper, a micromechanics-based elastic model is developed for two-phase FGMs, based on their zoned microstructures. In the microscopic scale, a RVE is constructed to simulate the graded microstructure. Direct pair-wise particle interactions are taken into account and the corresponding averaged strains in both phases are derived. The effective elastic properties of FGMs are then computed by solving the ordinary differential equations with respect to the spatial location in the FGM gradation direction. Due to the microstructural gradation, the model captures the gradient effect of phase volume fraction distribution. If the particle interaction terms are dropped, the model is reduced to the Mori–Tanaka's model. Comparisons are conducted among the present simulations and the available numerical simulation and experimental data to illustrate the performance of the proposed micromechanics framework.

## Acknowledgements

This work is sponsored by the National Science Foundation under grant numbers CMS-0084629 and CMS-0333576. The support is gratefully acknowledged.

## Appendix A

The coefficients  $c_i$  ( $i = 1, 2, \dots, 5$ ) that appear in Eq. (11) are defined as

$$c_1 = \frac{-d_1(2d_2 + 4d_4 + d_5) + d_3^2}{4d_2[d_1(3d_2 + 4d_4 + d_5) + d_2(2d_2 + 2d_3 + 4d_4 + d_5) - d_3^2]} + \frac{\alpha}{2\beta(3\alpha + 2\beta)},$$

$$c_2 = \frac{1}{4d_2} - \frac{1}{4\beta},$$

$$c_3 = \frac{-d_1(4d_4 + d_5) - 2d_2d_3 - d_3^2}{4d_2[d_1(3d_2 + 4d_4 + d_5) + d_2(2d_2 + 2d_3 + 4d_4 + d_5) - d_3^2]},$$

$$c_4 = -\frac{d_4}{4d_2(d_2 + d_4)},$$

$$c_5 = \left\{ d_2(8d_3d_4 + 3d_3^2 - 3d_1d_5 - 2d_2d_5 + 2d_4d_5 + 8d_4^2) + d_1d_4(4d_4 + d_5) - d_3^2d_4 \right\} / \left\{ 4d_2(d_2 + d_4) \times [d_1(3d_2 + 4d_4 + d_5) + d_2(2d_2 + 2d_3 + 4d_4 + d_5) - d_3^2] \right\},$$

where

$$d_1 = \alpha - \frac{\tilde{\rho}^3}{60\mu_0(1 - v_0)} (5 - 3\tilde{\rho}^2),$$

$$d_2 = \beta + \frac{\tilde{\rho}^3}{60\mu_0(1 - v_0)} (5 - 10v_0 + 3\tilde{\rho}^2),$$

$$d_3 = \frac{\tilde{\rho}^3}{4\mu_0(1 - v_0)} (1 - \tilde{\rho}^2),$$

$$d_4 = \frac{\tilde{\rho}^3}{4\mu_0(1 - v_0)} (v_0 - \tilde{\rho}^2),$$

$$d_5 = -\frac{\tilde{\rho}^3}{4\mu_0(1 - v_0)} (5 - 7\tilde{\rho}^2),$$

$$\alpha = -\frac{\lambda_1 - \lambda_0}{2(\mu_1 - \mu_0)[3(\lambda_1 - \lambda_0) + 2(\mu_1 - \mu_0)]} - \frac{1}{30\mu_0(1 - v_0)},$$

$$\beta = \frac{1}{4(\mu_1 - \mu_0)} + \frac{4 - 5v_0}{30\mu_0(1 - v_0)},$$

with  $\lambda_I, \mu_I$  being the Lamé constants for phase I ( $I = 0, 1$ ), respectively.

## References

- [1] Suresh S, Mortensen A. Fundamentals of functionally graded materials. IOM Communications Ltd; 1998.
- [2] Miyamoto Y, Kaysse WA, Rabin BH, Kawasaki A, Ford RG. Functionally graded materials: design, processing and applications. Dordrecht: Kluwer Academic Publishers; 1999.
- [3] Paulino GH, Jin ZH, Dodds RH. In: Karihaloo B, Knauss WG, editors. Comprehensive structural integrity, vol. 2; 2003. p. 607.
- [4] Ilshner B. J Mech Phys Solids 1996;44:647.
- [5] Aboudi J, Pindera M-J, Arnold SM. Composites Part B 1999;30:777.
- [6] Mori T, Tanaka K. Acta Metall 1973;21:571.
- [7] Hill R. J Mech Phys Solids 1965;13:213.
- [8] Budiansky B. J Mech Phys Solids 1965;13:223.
- [9] Zuiker JR. Compos Eng 1995;5:807.
- [10] Gasik MM. Comput Mater Sci 1998;13:42.
- [11] Vel SS, Batra RC. AIAA J 2002;40:1421.
- [12] Kim JH, Paulino GH. Inter J Numer Meth Eng 2003;58:1457.
- [13] Ju JW, Chen TM. Acta Mech 1994;103:123.
- [14] Sasaki M, Hirai T. J Ceram Soc Jap 1991;99:1002.
- [15] Hirano T, Teraki J, Yamada T. SMIRT 11 Transactions SDI 1991:49.
- [16] Reiter T, Dvorak GJ. J Mech Phys Solids 1998;46:1655.
- [17] Zuiker JR, Dvorak GJ. Compos Eng 1994;4:19.
- [18] Reiter T, Dvorak GJ, Tvergaard V. J Mech Phys Solids 1997;45:1281.
- [19] Grujicic M, Zhang Y. Mater Sci Eng A 1998;251:64.
- [20] Cho JR, Ha DY. Mater Sci Eng A 2001;302:187.
- [21] Eshelby JD. Proc Roy Soc A 1957;241:376.
- [22] Moschovidis ZA, Mura T. ASME J Appl Mech 1975;42:847.
- [23] Mura T. Micromechanics of defects in solids. 2nd ed. Dordrecht: Kluwer Academic Publishers; 1987.
- [24] Nemat-Nasser S, Hori M. Micromechanics: overall properties of heterogeneous materials. 2nd ed. Amsterdam: North-Holland; 1999.
- [25] Kröner E. In: Weng GJ, Taya M, Abé H, editors. Micromechanics and inhomogeneity; 1990. p. 197.
- [26] Ju JW, Sun LZ. Int J Solids Struct 2001;38:183.
- [27] Percus JK, Yevick GJ. Phys Rev 1958;110:1.
- [28] Eischen JW. Int J Fract 1987;34:3.
- [29] Bao G, Cai H. Acta Mater 1997;45:1055.
- [30] Zhai PC, Jiang CR, Zhang QJ. In: Holt JB, Kiozumi M, Hirai T, Munir ZA, editors. Ceramic transactions: functionally gradient materials. Westerville, OH: The American Ceramic Society; 1993. p. 449.
- [31] Parameswaran V, Shukla A. J Mater Sci 2000;35:21.